Geophysical Research Letters

RESEARCH LETTER
10.1029/2023GL108066

Evidence for SSW Triggered Q6DW-Tide and Q6DW-Gravity Wave Interactions Observed by Meteor Radars at 30°S

Zishun Qiao[1,2], Alan Z. Liu[1], N. M. Pedatella[2], Gunter Stober[3], Iain M. Reid[4,5], Javier Fuentes[6], and Christian L. Adami[4]

[1]Center for Space and Atmospheric Research and Department of Physical Sciences, Embry-Riddle Aeronautical University, Daytona Beach, FL, USA, [2]High Altitude Observatory, NSF National Center for Atmospheric Research, Boulder, CO, USA, [3]Institute of Applied Physics & Oeschger Center for Climate Change Research, Microwave Physics, University of Bern, Bern, Switzerland, [4]ATRAD Pty. Ltd., Thebarton, SA, Australia, [5]School of Physical Sciences, University of Adelaide, Adelaide, SA, Australia, [6]European Southern Observatory, Santiago, Chile

Abstract An exceptionally strong westward propagating quasi-6-day wave (Q6DW) with zonal wavenumber 1 in connection with the rare 2019 Southern Hemispheric Sudden Stratospheric Warming (SSW) is observed by two meteor radars at 30°S and is found to modulate and interact with the diurnal tide and gravity waves (GWs). The diurnal tide is amplified every 6 days and a prominent 21 hr child wave attributed to Q6DW-diurnal tide nonlinear interaction occurs. Q6DW modulation on GWs is confirmed as the 4–5 day periodicity in GW variances. Simultaneously, the Q6DW appears to shift its period toward the periodicity of the modulated GW variances. Enhancement is also observed in the first results of meteor radar observed Q6DW Eliassen-Palm flux, which may facilitate the global perturbation and persistence of this Q6DW. We conclude that the observed SSW triggered Q6DW-tide and Q6DW-GW interactions play an important role in coupling the lower atmospheric forcings to ionospheric variabilities.

Plain Language Summary Our work provides observational evidence for the 6-day planetary wave-tide and 6-day planetary wave-gravity wave interactions at the Earth's mesosphere and lower thermosphere. The results strongly support the theory that wave-wave interactions are the primary mechanism coupling planetary waves to ionospheric variability and provide an additional mechanism as the 6-day wave modulation on the gravity waves. We utilize measurements from two meteor radars to diagnose planetary wave characteristics and identify wave-wave interactions, and compute the first-time meteor radar observed Eliassen-Palm flux. Enhancement is observed in the Eliassen-Palm flux of 6-day wave following the SSW maximum phase, which demonstrates that energy of the 6-day wave is enhanced and therefore, facilitates the global perturbation and persistence of the 6-day wave for an extended time period. While meteor radar observations are widely used to investigate planetary waves and tides, high meteor detection rate is required for further studying temperature perturbations and small scale waves (e.g., gravity waves). Thus, this work also highlights the capability of a modern multi-static meteor radar system, Chilean Observation Network De meteOr Radars, in resolving oscillations of small spatial scales over a broad range of periods, and for calculating Eliassen-Palm flux of planetary waves.

Key Points:

- A dominating W1 Q6DW is observed at 30°S and its Eliassen-Palm flux is enhanced during the 2019 SH SSW
- Q6DW amplifies the diurnal tide every 6 days and a strong 21 hr child wave is observed
- Q6DW modulates the gravity wave variances and its frequency appears to shift accordingly

Supporting Information:

Supporting Information may be found in the online version of this article.

Correspondence to:

Z. Qiao and A. Z. Liu,
qiaoz1@my.erau.edu;
liuz2@erau.edu

Citation:

Qiao, Z., Liu, A. Z., Pedatella, N. M., Stober, G., Reid, I. M., Fuentes, J., & Adami, C. L. (2024). Evidence for SSW triggered Q6DW-tide and Q6DW-gravity wave interactions observed by meteor radars at 30°S. *Geophysical Research Letters*, *51*, e2023GL108066. https://doi.org/10.1029/2023GL108066

Received 28 JAN 2024
Accepted 15 MAR 2024

1. Introduction

The Sudden Stratospheric Warming (SSW) is a major anomaly in the winter stratosphere that have been extensively studied (see e.g., Baldwin et al., 2021, and references there in). The mechanism for the generation of SSWs is described by Matsuno (1971) as the vertical propagation of planetary waves (PWs) and their interaction with the zonal mean flow. SSWs occur primarily in the Northern Hemisphere (NH) during winter seasons and are rare in the Southern Hemisphere (SH). The relatively quick succession of two SH SSWs in 2002 and 2019 will likely remain special in history, since the frequency of SH SSWs is about once in 22 years and is expected to become much rarer under future climate change (Jucker et al., 2021). The impact of SSW is not confined in the stratosphere, but often leads to major disturbances in the mesosphere and lower thermosphere (MLT) region (e.g., Gasperini et al., 2022; Jones et al., 2020; Oberheide et al., 2020). Understanding how the rare SH SSWs influence the upper atmosphere is therefore an important topic to investigate.

AGU ADVANCING EARTH AND SPACE SCIENCES

Geophysical Research Letters

RESEARCH LETTER
10.1029/2023GL108066

Evidence for SSW Triggered Q6DW-Tide and Q6DW-Gravity Wave Interactions Observed by Meteor Radars at 30°S

Zishun Qiao[1,2], Alan Z. Liu[1], N. M. Pedatella[2], Gunter Stober[3], Iain M. Reid[4,5], Javier Fuentes[6], and Christian L. Adami[4]

[1]Center for Space and Atmospheric Research and Department of Physical Sciences, Embry-Riddle Aeronautical University, Daytona Beach, FL, USA, [2]High Altitude Observatory, NSF National Center for Atmospheric Research, Boulder, CO, USA, [3]Institute of Applied Physics & Oeschger Center for Climate Change Research, Microwave Physics, University of Bern, Bern, Switzerland, [4]ATRAD Pty. Ltd., Thebarton, SA, Australia, [5]School of Physical Sciences, University of Adelaide, Adelaide, SA, Australia, [6]European Southern Observatory, Santiago, Chile

Key Points:

- A dominating W1 Q6DW is observed at 30°S and its Eliassen-Palm flux is enhanced during the 2019 SH SSW
- Q6DW amplifies the diurnal tide every 6 days and a strong 21 hr child wave is observed
- Q6DW modulates the gravity wave variances and its frequency appears to shift accordingly

Supporting Information:

Supporting Information may be found in the online version of this article.

Correspondence to:

Z. Qiao and A. Z. Liu,
qiaoz1@my.erau.edu;
liuz2@erau.edu

Citation:

Qiao, Z., Liu, A. Z., Pedatella, N. M., Stober, G., Reid, I. M., Fuentes, J., & Adami, C. L. (2024). Evidence for SSW triggered Q6DW-tide and Q6DW-gravity wave interactions observed by meteor radars at 30°S. *Geophysical Research Letters*, *51*, e2023GL108066. https://doi.org/10.1029/2023GL108066

Received 28 JAN 2024
Accepted 15 MAR 2024

Abstract An exceptionally strong westward propagating quasi-6-day wave (Q6DW) with zonal wavenumber 1 in connection with the rare 2019 Southern Hemispheric Sudden Stratospheric Warming (SSW) is observed by two meteor radars at 30°S and is found to modulate and interact with the diurnal tide and gravity waves (GWs). The diurnal tide is amplified every 6 days and a prominent 21 hr child wave attributed to Q6DW-diurnal tide nonlinear interaction occurs. Q6DW modulation on GWs is confirmed as the 4–5 day periodicity in GW variances. Simultaneously, the Q6DW appears to shift its period toward the periodicity of the modulated GW variances. Enhancement is also observed in the first results of meteor radar observed Q6DW Eliassen-Palm flux, which may facilitate the global perturbation and persistence of this Q6DW. We conclude that the observed SSW triggered Q6DW-tide and Q6DW-GW interactions play an important role in coupling the lower atmospheric forcings to ionospheric variabilities.

Plain Language Summary Our work provides observational evidence for the 6-day planetary wave-tide and 6-day planetary wave-gravity wave interactions at the Earth's mesosphere and lower thermosphere. The results strongly support the theory that wave-wave interactions are the primary mechanism coupling planetary waves to ionospheric variability and provide an additional mechanism as the 6-day wave modulation on the gravity waves. We utilize measurements from two meteor radars to diagnose planetary wave characteristics and identify wave-wave interactions, and compute the first-time meteor radar observed Eliassen-Palm flux. Enhancement is observed in the Eliassen-Palm flux of 6-day wave following the SSW maximum phase, which demonstrates that energy of the 6-day wave is enhanced and therefore, facilitates the global perturbation and persistence of the 6-day wave for an extended time period. While meteor radar observations are widely used to investigate planetary waves and tides, high meteor detection rate is required for further studying temperature perturbations and small scale waves (e.g., gravity waves). Thus, this work also highlights the capability of a modern multi-static meteor radar system, Chilean Observation Network De meteOr Radars, in resolving oscillations of small spatial scales over a broad range of periods, and for calculating Eliassen-Palm flux of planetary waves.

1. Introduction

The Sudden Stratospheric Warming (SSW) is a major anomaly in the winter stratosphere that have been extensively studied (see e.g., Baldwin et al., 2021, and references there in). The mechanism for the generation of SSWs is described by Matsuno (1971) as the vertical propagation of planetary waves (PWs) and their interaction with the zonal mean flow. SSWs occur primarily in the Northern Hemisphere (NH) during winter seasons and are rare in the Southern Hemisphere (SH). The relatively quick succession of two SH SSWs in 2002 and 2019 will likely remain special in history, since the frequency of SH SSWs is about once in 22 years and is expected to become much rarer under future climate change (Jucker et al., 2021). The impact of SSW is not confined in the stratosphere, but often leads to major disturbances in the mesosphere and lower thermosphere (MLT) region (e.g., Gasperini et al., 2022; Jones et al., 2020; Oberheide et al., 2020). Understanding how the rare SH SSWs influence the upper atmosphere is therefore an important topic to investigate.

During the 2019 SH SSW event, presence of enhanced traveling PW activities throughout the atmosphere were reported (e.g., He et al., 2020; G. Liu et al., 2021; Lee et al., 2021; Ma et al., 2022; Wang et al., 2021) and are believed to have induced significant ionospheric variabilities (e.g., Goncharenko et al., 2020; Yamazaki et al., 2020). In particular, prominent quasi-6-day periodicities in the equatorial electrojet (EEJ) were observed and attributed to the quasi-6-day wave (Q6DW) simultaneously observed in the middle atmosphere (Yamazaki et al., 2020). However, the possible processes that are responsible for generating the 6-day ionospheric variability in connection with the large Q6DW remain unclear. The 6-day ionospheric variability may be due to direct impact of PWs that propagate above 100 km, or due to the PW modulation of tides and gravity waves (GWs) that carry the PW periodicities into the ionosphere.

Observations have confirmed that the PWs modulation on tides and their nonlinear interactions are key mechanisms that couple SSW to ionospheric variabilities (Pedatella & Forbes, 2010). Numerical simulations indicate that the 6-day planetary wave can produce similar oscillations in the ionosphere, through both primary and secondary waves resulting from Q6DW-tides interactions (Forbes & Zhang, 2017; Gan et al., 2017; Pedatella et al., 2012). However, investigations of wave-wave interactions across the scales of PW, tides, and in particular, gravity waves remain insufficient, despite the fact that the modulations of GWs could produce important ionospheric variabilities (H.-L. Liu, 2016). This lack of understanding wave-wave interactions across all scales is particularly challenged by small scale waves (i.e., GWs) due to observational constraints. Observations from Sun-synchronous and quasi-Sun-synchronous satellites (e.g., Forbes & Zhang, 2017), or meteor radar data from observing stations located at the same latitude (e.g., He et al., 2017, 2018, 2020), can be analyzed to reveal the signatures of nonlinear interactions between tides and PWs. However, existing satellite observations are not suitable to study interactions involving GWs due to their relatively low temporal resolution. Leveraging observations of co-located lidar and meteor radar could contribute to understanding interactions between GWs and large-scale waves as presented in A. Z. Liu et al. (2013), but is still limited to climatological time scales. The estimation of GW variances and momentum fluxes from meteor radars were previously discussed with an emphasis on the high temporal (hourly, daily) and spatial resolutions (e.g., R. J. De Wit et al., 2014; Stober, Janches, et al., 2021) or on the performance of long temporal averages (monthly mean) (e.g., R. De Wit et al., 2016, 2017; Fritts et al., 2012) employing the method proposed by W. Hocking (2005). Chilean Observation Network De meteOr Radars (CONDOR), a recently deployed multi-static meteor radar system operating with a high transmitting power, that is, high meteor detection rates, can significantly improve the estimation of GW variances and momentum fluxes (Conte et al., 2022; Stober, Kozlovsky, et al., 2021; Stober et al., 2022). High resolution GW variance and momentum flux measurements further facilitate the examination of short-term PW-tide-GW interactions, which is inherently connecting the lower atmospheric forcing to the E-region dynamo related ionospheric periodicities (e.g., Gan et al., 2016).

The 2019 SH SSW presents a unique case in that the Q6DW was particularly strong and dominant (Lee et al., 2021; G. Liu et al., 2021), thus providing ideal conditions to investigate the nonlinear interactions between the Q6DW, tides, and GWs. Although simulation work explained the excitation mechanism of the ionospheric 6-day periodicity during the 2019 SH SSW as the superposition of secondary waves from Q6DW-tide interactions (Miyoshi & Yamazaki, 2020), there is a lack of discussion on the role of gravity waves, as well as direct observational confirmation of Q6DW-wave nonlinear interactions. In the present study we use observations from two meteor radars at 30°S to determine the characteristics of the Q6DW, and specifically utilize CONDOR measurements to present the first observational evidence of Q6DW-tide and Q6DW-GW interactions in the MLT during the 2019 SH SSW. We further present the first-time meteor radar observed Eliassen-Palm (E-P) flux of the Q6DW.

2. Data and Methods

The current work investigates Q6DW-tide and Q6DW-GW interactions using MLT zonal and meridional winds and temperatures from observations of two meteor radars (MRs). Specifically, winds from the remote site of Buckland Park MR (35.1°S, 138.8°E), and winds and temperatures from CONDOR/SCO site (31.2°S, 71.0°W) are utilized. Characteristics and some results of CONDOR can be found in Stober, Kozlovsky, et al. (2021), Stober et al. (2022), and Conte et al. (2022) and those of Buckland Park MR are described in Spargo et al. (2019) and Holdsworth et al. (2004), and are not repeated herein. In addition to CONDOR measured horizontal winds, GW variances (or wind variances, u'^2, v'^2, w'^2) and momentum fluxes ($u'v'$, $u'w'$, $v'w'$) contained in the Reynolds stress components (where u', v', w' refers to the fluctuating eastward, northward, and vertical winds) are

computed by a recently developed 3DVAR+DIV algorithm. This algorithm creates a tomographic reconstruction of the 3D wind field based on optimal estimation technique and Bayesian statistics as well as GW momentum fluxes and variances, and has been adapted to CONDOR measurements (Stober, Kozlovsky, et al., 2021; Stober et al., 2022). The Reynolds stress components (i.e., GW momentum fluxes and variances) are derived from Reynolds-averaged Navier-Stokes equations based on the method suggested by W. Hocking (2005) and the detailed retrieval can be found in Stober, Janches, et al. (2021). Meteor detection rate of CONDOR is particularly increased by its 48 kW high power transmitter that leads to roughly 30,000 valid detections per site per day. Such sufficient data set controls the uncertainties of 3DVAR+DIV estimations, and also improves the resolution of temperature analysis. The background atmospheric temperature at the peak height of meteor detections has the following relationship with the ambipolar diffusion coefficient of the meteor plasma trails (W. K. Hocking, 1999; W. K. Hocking et al., 1997)

$$T = S \cdot \log_{10} e \cdot \left(2\frac{dT}{dz} + \frac{mg}{k}\right), \tag{1}$$

where T is the temperature we are aiming to compute from radar observations; e is the Euler's number; m is the molecular weight of the air; g is the gravity acceleration and k is the Boltzmann constant. dT/dz is the vertical temperature gradient and is calculated based on temperature profiles from MSIS (Hedin, 1991). Seasonal variations are retained in the MSIS temperature gradient but not the day-to-day variabilities. S is computed by performing a robust regression to the linear model of $z = S \cdot \log_{10} D_a + c$, where z is height, D_a is the measured ambipolar diffusion coefficient of meteor trail plasma and c is a constant. Daily temperatures with a vertical resolution of 2 km are derived from meteor detections peaking at different heights with an artificially selected Gaussian distribution (mean μ = peak height, standard deviation σ = 4 km). Specifically, only the underdense meteor detections are considered (e.g., Kaiser & Closs, 1952; Stober, Brown, et al., 2021) and the potential polarization effects are mitigated by utilizing detections with zenith angle less than 50°. The outlier effects in linear regression are reduced by limiting the probability density from kernel density estimation, and performing robust regression. Similar temperature derivation method has also been explained in previous studies (e.g., Stober et al., 2008; Yi et al., 2016) and it is noted that the temporal resolution of meteor radar temperatures is suitable for resolving planetary wave-scale oscillations (Stober et al., 2012).

To understand the effects of the Q6DW on the zonal mean flow, we calculated its *local* quasi-geostrophic Eliassen-Palm (E-P) flux (Andrews & McIntyre, 1976; Eliassen & Palm, 1961) using the observed temperatures and winds. The E-P flux vector is defined as $\boldsymbol{F} = \boldsymbol{j}F_y + \boldsymbol{k}F_z$ where the meridional and vertical components are respectively

$$\begin{aligned} F_y &= -\langle u'v' \rangle, \\ F_z &= \frac{gf}{N^2}\frac{\langle \theta'v' \rangle}{\langle \theta \rangle}, \end{aligned} \tag{2}$$

where N, g, f, u, v, θ denote buoyancy frequency, gravitational acceleration, Coriolis parameter, zonal and meridional wind, and potential temperature, respectively. The brackets represent the zonal average and the primes represent planetary wave perturbations relative to the zonal average. In this work, temporal instead of zonal average are used with the assumption that the identified W1 Q6DW is unambiguously isolated by the meteor radar measurements at a single location. The perturbation in the zonal wind of a sinusoidal wave can be expressed as $u' = \Re\{\tilde{u}e^{i(\omega t - kx)}\}$, where $\tilde{u} = u_0 e^{i\phi_u}$ (u_0 and ϕ_u are the real amplitude and phase, respectively) is the complex amplitude, ω is the angular frequency, k is the wave number, and $\Re$ represents the real part. Then the momentum flux and the heat flux, obtained by averaging either over t or x for one wave period or one wavelength, are

$$\begin{aligned} \langle u'v' \rangle &= \overline{u'v'} = \frac{1}{2}\Re\{\tilde{u}\tilde{v}^*\} = \frac{1}{2}\Re\left\{u_0 v_0 e^{i(\phi_u - \phi_v)}\right\}, \\ \langle \theta'v' \rangle &= \overline{\theta'v'} = \frac{1}{2}\Re\left\{\tilde{\theta}\tilde{v}^*\right\} = \frac{1}{2}\Re\left\{\theta_0 v_0 e^{i(\phi_\theta - \phi_v)}\right\}, \end{aligned} \tag{3}$$

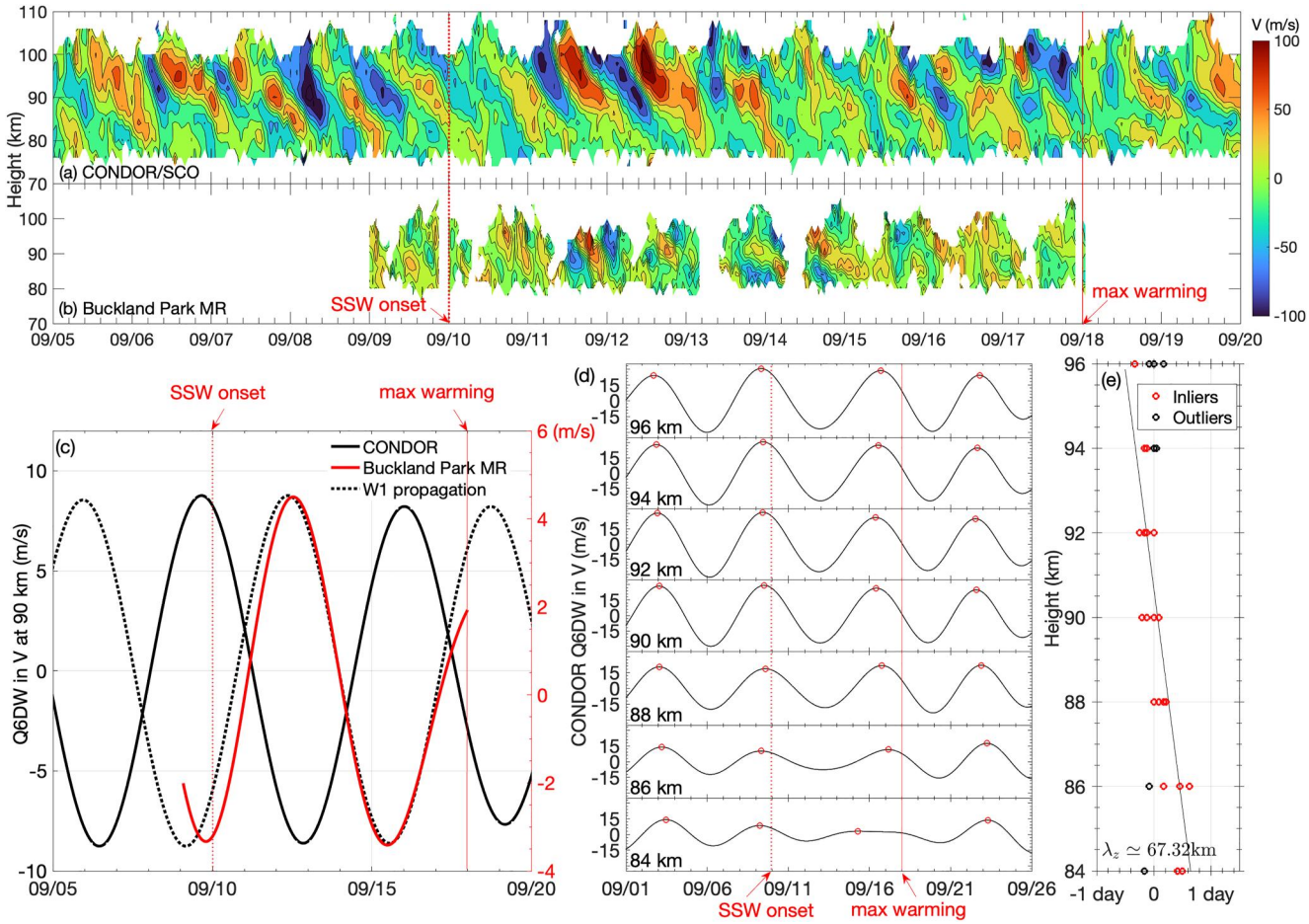

Figure 1. (a, b) CONDOR/SCO and Buckland Park MR meridional winds at 70–110 km from September 05 to September 20. (c) Amplitudes of the fitted Q6DW at 90 km in CONDOR (black solid line) and Buckland Park MR (red solid line) meridional winds are presented in the left and right axes, respectively. The black dotted line denotes the shifted (150.2°/360° × 6.5 days) CONDOR results to Buckland Park MR assuming a zonal wavenumber 1 propagation. (d) Q6DW in CONDOR meridional winds at 84–96 km. Peaks of the Q6DW denote the sinusoidal wave phases of 90° and are marked by the red circles. Red vertical lines in (a–d) denote the SSW onset (09/10, dotted) and the maximum warming time (09/18, solid). (e) The robust fitted slope (height difference/phase difference) multiplying 6.5 days period indicates the vertical wavelength of ∼67.3 km. Note that the inliers (red) and outliers (black) are detected by robust regression.

where the overbar denotes the temporal average. The complex amplitudes and phases of u', v', and θ' are obtained from Morlet wavelet analysis, and the superscript * indicates complex conjugate. Note that $T'/\bar{T}$ is used to approximate $\theta'/\langle\theta\rangle$ since the relative pressure perturbations in planetary waves are much smaller than the relative temperature perturbations.

3. Results and Discussion

Prior to the onset of, during, and after the 2019 SH SSW in September 2019, CONDOR winds show significantly enhanced quasi-6-day wave activity. For comparison, Q6DW activities in CONDOR winds are also analyzed for September 2020 and 2021, and it is apparent that Q6DW activity in 2019 is much stronger and thus most likely related to this rare SSW event (not shown). As described earlier, we use two meteor radar wind measurements, CONDOR and Buckland Park MR, which are at about the same latitude (30°S) but longitudinally separated by 150.2°, to diagnose the characteristics of this Q6DW. In Figure 1, the top two panels present the meridional winds observed by CONDOR/SCO site (Figure 1a) and Buckland Park MR (Figure 1b), while the zonal wind measurements have been included in Figure S1. The left panel (Figure 1c) shows quasi-6-day oscillations of meridional wind at 90 km from CONDOR and Buckland Park MR in September 2019. The Q6DW oscillations shown in Figure 1c are obtained by least squares fitting the meteor radar winds to the form $A_0 + \sum_{i=1}^{3} A_i \cos\left(2\pi t/T_i - \phi_i\right)$, where the first term A_0 represents the background wind and the second term

denotes the fitted Q6DW. A_i and ϕ_i are the amplitude and phase of the Q6DW, t is universal time unit in days, and $T_{1,2,3}$ ($\simeq$ 5.88, 6.30, 6.76 days) are known periods in the range of 5.5–7 days obtained from Morlet wavelet analysis on CONDOR winds only. It is assumed that the Q6DW has same frequency at two radar locations, since the short temporal coverage (10 days) of Buckland Park MR winds limits the spectrum analysis of the Q6DW. Note that the Q6DW amplitude is larger at CONDOR, and the wind perturbations are plotted with different vertical scales to facilitate easier comparison of their phase difference. The difference in wave amplitudes may be related to the Q6DW being affected by other longitudinally variable waves such as the orographic gravity waves (Lieberman et al., 2013; McLandress & McFarlane, 1993). The black dotted line (Figure 1c) is the CONDOR wind perturbation shifted to Buckland Park MR assuming it is a zonal wavenumber 1 structure propagating westward at a peak period of 6.5 days. The time shift between the black dotted line and black solid line is computed as 150.2°/360° × 6.5 days, where 150.2° is the longitudinal difference of these two radars. The agreement between the black dotted line and the red solid line is thus consistent with the Q6DW being a westward propagating wave with wavenumber 1. The middle panel (Figure 1d) shows the Q6DW in CONDOR meridional winds identified by Morlet wavelet analysis (in the same 5.5–7 day period range) at various altitudes, with their peaks marked by red dots. The right panel (Figure 1e) shows the times of the peaks relative to the peaks of a 6.5-day wave at 90 km (red dots) and a robust linear fit with altitude. The slope of this fitted line indicates that the vertical wavelength of this wave is about 67.3 km, consistent with previous findings that the 6-day planetary wave has a long vertical wavelength of ∼60–70 km (e.g., Forbes & Zhang, 2017; Lieberman et al., 2003).

Having determined the characteristics of the enhanced Q6DW, we now turn our attention to its modulations and interactions with tides and GWs. Figure 2 presents the continuous 1-D wavelet transform spectrum of zonal and meridional winds, temperatures, tidal amplitudes, and GW variances from CONDOR measurements at 90 km. In particular, Figures 2b and 2d show the absolute wave amplitudes (absolute value of the magnitudes from Morlet wavelet transform) while Figures 2a, 2c, 2e, and 2f plot the wave signals (real part of the magnitudes from Morlet wavelet transform). Q6DW spectrum in V, U, T is shown in Figures 2a, 2c, and 2e, and the Q6DW signals (the sum of wavelet wave signals in the range of 4–7 days, note it is not scaled to the peak value) are presented by the solid (V), dashed (U), and dotted lines (T), respectively. Different wave modulations and interactions appear at different times and are separated by the vertical line, which indicates when the 2019 SH SSW reaches the maximum warming time (Mitra et al., 2022) and the wind reversal region descended to lower altitudes of ∼40 km (Yamazaki et al., 2020). Before September 18, it is apparent that the Q6DW activity is dominant in meridional wind, as indicated by the 4–7 days peaks in wave spectrum (Figure 2a). The Q6DW clearly modulates the diurnal tide, where the amplitude of diurnal tide is amplified every 6 days and reaches 40–60 m/s (Figure 2b). This is supported by the theory that the PW-tide nonlinear interaction can modulate the tidal amplitude with a period equal to the planetary wave period (Teitelbaum & Vial, 1991). Evidence of Q6DW-diurnal tide nonlinear interaction is further confirmed by the occurrence of a 21 hr wave around September 21 with an amplitude in excess of 60 m/s in the meridional wind (Figure 2b), which is the secondary wave (also known as child wave) of Q6DW-diurnal tide interaction (Teitelbaum & Vial, 1991). Considering the spread in time and frequency in wavelet spectra introduced by the wavelet filters, the 21 hr wave is determined as evident here only if its amplitude is large (>40 m/s) and apparently surpasses the diurnal tide amplitude (>30% difference). Separate Fast Fourier Transform analysis of the meridional winds, which provides finer spectral resolution than the wavelets analysis, confirms the presence of a 21 hr wave (not shown). Note that the amplitude of Q6DW in meridional wind is further enhanced after September 21, which can be excited by the presented 21 hr secondary wave in-turn nonlinearly interacting with the diurnal tide. This could be a possible Q6DW excitation mechanism in the MLT region during this SH SSW. These results indicate that the Q6DW-diurnal tide interaction occurs at an early stage and persists throughout the 2019 SH SSW, which is possibly connected to the 6-day periodicity observed in the equatorial electrojet (EEJ) and electron density (Yamazaki et al., 2020). This mechanism is supported by Gan et al. (2017), in which the 21 and 13 hr child waves associated with the Q6DW-diurnal/semidiurnal tide nonlinear interactions in the E region were found to be most responsible for the 6-day variations in the ionosphere. The presented 21 hr child wave also confirms the results of Pedatella et al. (2012) that the 20–24 hr wave produced by Q6DW-diurnal tide nonlinear interaction achieves the largest amplitude among the child waves. Although simulations connected the ionospheric 6-day periodicity primarily to Q6DW-semidiurnal tide nonlinear interactions at 43°N during this SSW (Miyoshi & Yamazaki, 2020), neither the 13 hr nor 11 hr secondary wave was significant in the present observations at 30°S. However, relatively small amplitude 21 hr wave was notable in the simulations near 1°N (Miyoshi & Yamazaki, 2020), which suggests an interhemispheric asymmetry of the

10.1029/2023GL108066

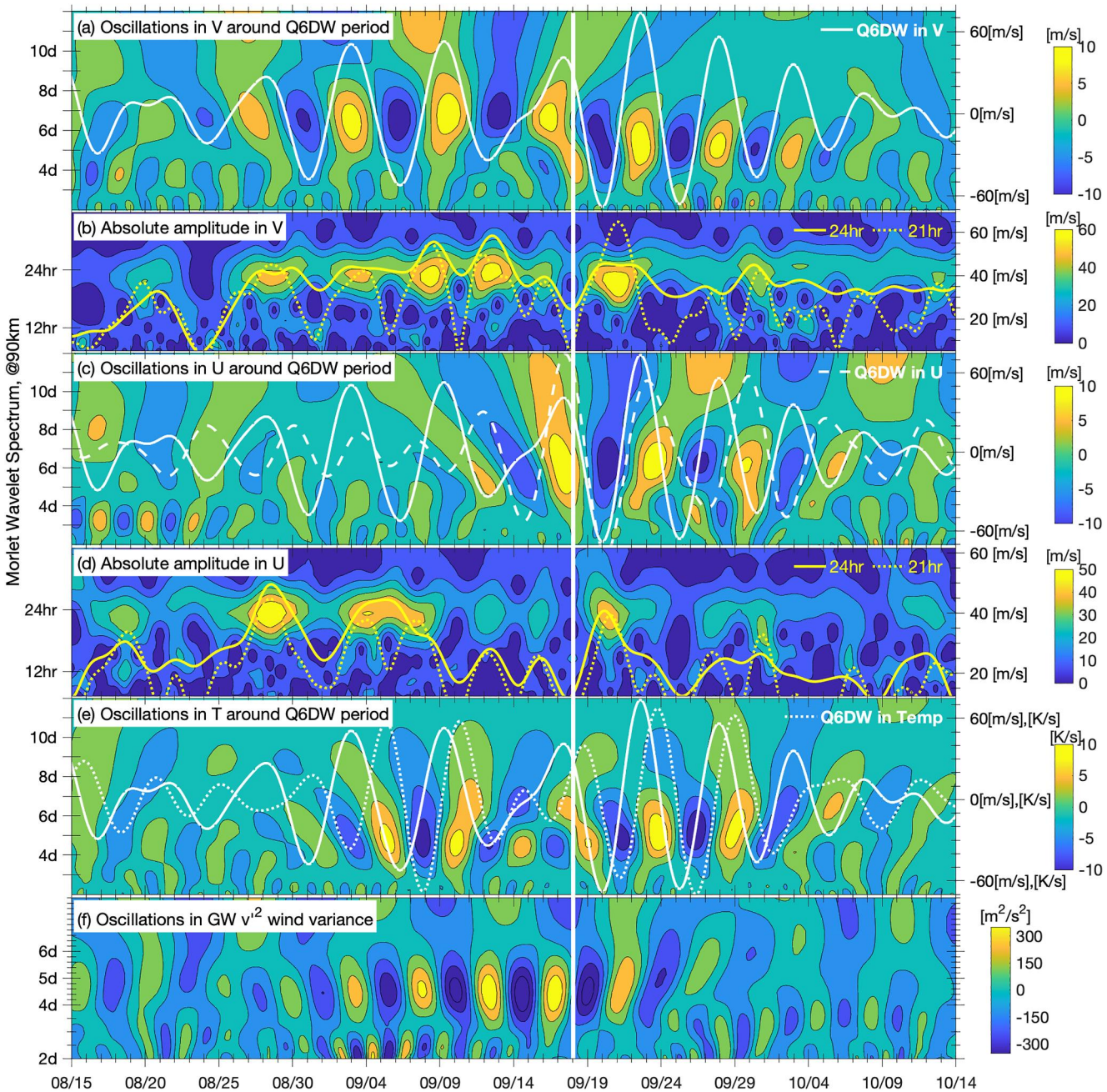

Figure 2. Morlet wavelet spectrum of Q6DW in (a) V, (c) U, (e) T; Diurnal tide amplitude in (b) V and (d) U; (f) GW variance in meridional wind. The Q6DW (4–7 days) signals in V (white solid line), V and U (white dashed line), and V and T (white dotted line) are overlayed in (a, c, e), respectively. Amplitudes of diurnal tide (yellow solid line) and 21 hr child wave (yellow dotted line) are overlayed in (b, d). All panels are at 90 km from CONDOR observations. The vertical line denotes the SSW maximum warming time.

Q6DW-tide interactions. Such asymmetry could be attributed to the seasonal hemispheric differences in dominating tides (e.g., Stober, Kuchar, et al., 2021).

We now discuss the Q6DW modulation and interaction with the GWs. Figure 2f presents the wavelet spectrum of GW variances in CONDOR meridional wind at 90 km. Of particular interest is the GW variances oscillating with a 4–5 days periodicity between September 05–20 (Figure 2f) and this oscillation peaking around the same time when the peak period of the Q6DW shifts from 6–7 days to 4–6 days (Figure 2a). These simultaneous observations of the Q6DW and the 4–5 days periodicity in GW variances present direct confirmation of Q6DW

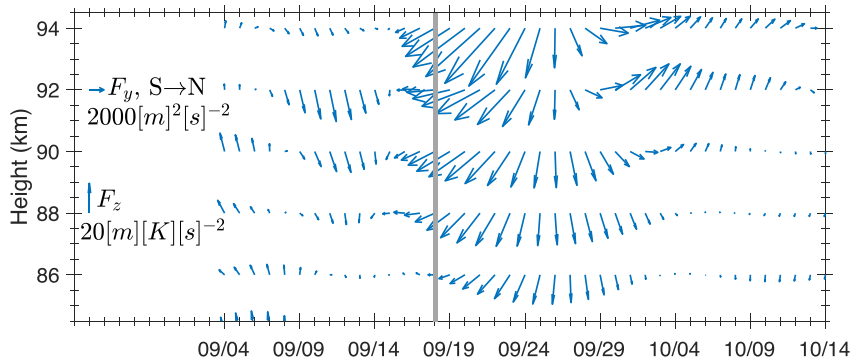

Figure 3. Time-averaged Q6DW E-P flux vectors from September 4 to October 14, at 86–94 km, ∼30°S, derived from CONDOR winds and temperatures. Scale vectors are indicated on the left side and the vertical gray line denotes the SSW maximum warming time. Please note that the E-P flux vectors here are plotted as height versus time, rather than the common meridional cross section (i.e., the latitude-height plane).

modulation on GWs, and provide an additional mechanism of producing the reported ionospheric 6-day variability (Meyer, 1999). Although the Q6DW is not expected to directly propagate into the ionosphere, Q6DW modulated GWs can impact the upper atmosphere and produce the 6-day periodicity (Goncharenko et al., 2020; H.-L. Liu, 2016). It is possible that the weakening of eastward zonal mean zonal winds may result in the Doppler shifted Q6DW varying from longer to shorter periods. However, Geisler and Dickinson (1976) indicated that the effect of zonal wind on 5-day normal mode period tend to be small (<0.5 days) due to the cancellation of lower boundary temperature gradient influence. Though the reported Q6DW could be produced by atmospheric instability and distinct from the normal mode (Lieberman et al., 2003; Meyer & Forbes, 1997), the MLS geostrophic zonal mean zonal winds at this period of time weakens before Sep. 08 and strengthens after then (not shown), which does not align with the discussed Q6DW frequency shift. The relationship between the 4–5 days periodicity of GW variances and the *frequency shift* of the Q6DW in meridional wind around Sep. 18 is thus interesting but uncertain due to the limited fundamental understanding of GW-PW interactions. Specifically, *whether or not* and the *degree* to which changes in the GW day-to-day variability influences the Q6DW period is presently unclear and additional studies are necessary to fully understand this relationship. Systematic simultaneous observations of PW and GW activities on the day-to-day basis would contribute demonstrating the mechanism of PW-GW interactions. Supposing the above mechanism of PW-GW interaction is responsible for shifting the peak periods of the Q6DW, we may therefore expect to observe similar day-to-day variability of GWs in similar PW events. Frequency shift of planetary waves during SSWs was also found to occur by Yamazaki and Matthias (2019). They found a shift from either longer to shorter period or shorter to longer period, though the mechanism remained unclear. Based on the above, these results demonstrate the importance of investigating the influence of planetary waves on GW variability in future studies, which in-turn may lead to a frequency shift of the planetary waves. In addition, the phase of the Q6DW in meridional wind also shifted simultaneously with the frequency shift, which leads to the later in-phase relationships of V and U, and V and T, respectively (white lines in Figures 2c and 2e). These results could be interpreted as the absolute amplitude of momentum flux and heat flux of the Q6DW are enhanced during this time, and will be discussed in more detail later.

If both heat and momentum fluxes of the Q6DW are enhanced after the SSW maximum, the question remains as to which region is going to be perturbed by the energy carried in this wave packet. Figure 3 shows the *local* E-P flux vectors ($\boldsymbol{F}$) of this Q6DW at 86–94 km from September 4 to October 14, computed from CONDOR wind and temperature measurements by utilizing the aforementioned time-averaged method. Note that the Q6DW amplitude for calculating E-P flux is computed as the sum of wavelet wave signals in the range of 4–7 days, which may not be used to reconstruct the realistic amplitude and thus only the direction of $\boldsymbol{F}$ and the relative size of F_y and F_z are discussed. The direction of $\boldsymbol{F}$ determines the relative importance of the eddy fluxes of heat and momentum (Andrews & McIntyre, 1976; Eliassen & Palm, 1961). In the case of the present Q6DW, $\boldsymbol{F}$ is also a measure of net wave propagation from one height and latitude to another (e.g., Edmon et al., 1980). The meridional flux of zonal momentum dominates when the E-P flux vectors point in the meridional directions. Poleward F_y occurs from September 16 to 23 and its amplitude appears to increase with height. Several days later relatively small equatorward F_y is present around September 29 and, remains elevated for about 1 week. When

E-P flux vectors point more upward or downward the meridional heat flux dominates. Since September 16 downward F_z appears to be increased and then decreased over the period of two weeks at 86–94 km, and the latter part is relatively independent of height. F_z changes its direction to upward after September 30 and lasts for about 10 days, with a notable dependence on height (its greatest value is at ∼92 km). The overall amplitude enhancement of the E-P flux vectors around September 18 (SSW max) suggests energy exchange between the mean flow and the Q6DW, notably mainly exerting influences on the region above ∼90 km. Further investigation on the source of energy and the underlying mechanism is limited by the single location observation. These enhancements following the SSW maximum phase will, therefore, facilitate the global perturbation of the Q6DW, which could contribute to the persistence of the Q6DW for an extended time period following the SSW warming period September 10–20, as described in Mitra et al. (2022).

Although it was a minor warming, the 2019 Antarctic SSW produced even more ionospheric disturbances compared to Arctic events (Goncharenko et al., 2020). Of particular interest is the globally observed and persistent ionospheric quasi-6-day periodicity (e.g., Goncharenko et al., 2020; Yamazaki et al., 2020). Lower atmospheric forcing from the Q6DW-wave modulations and interactions could be responsible for producing the ionospheric 6-day periodicity, due to the indirect vertical penetration of the Q6DW into the ionosphere (e.g., Forbes & Zhang, 2017; Gan et al., 2017; Pedatella et al., 2012). The presented strong 6-day amplification of the diurnal tides can be related to the large longitudinal differences in PW oscillations observed by Goncharenko et al. (2020), though the decomposition of the DW1, DE2, and DE3 tides appears to be difficult to approach (not shown) in the current study. Evidence of the Q6DW-diurnal tide nonlinear interaction is found as a strong 21 hr child wave is observed, which suggests an interhemispheric asymmetry of the Q6DW-tide interactions since the 13 hr child wave from Q6DW-SW2 interaction was dominant near 43°N in simulations (Miyoshi & Yamazaki, 2020). Furthermore, the quasi-6-day periodicity in GW variances in the meridional wind suggests that the ionospheric quasi-6-day variability could also be attributed to the Q6DW-modulated GW propagating to the ionosphere and causing the ionospheric effects. In addition, the observed enhancement of the Q6DW E-P flux following the warming period could facilitate the global perturbation of the Q6DW for an extended time period.

4. Conclusions

In the present letter we analyze the enhanced and dominating W1 Q6DW activity and its nonlinear interactions with tides and GWs at SH mid-latitudes triggered by the rare 2019 SH SSW. The main conclusions of this letter are listed below:

1. The observations reveal significant quasi-6-day periodicities in both GW variances and diurnal tide amplitudes, providing clear evidence of Q6DW-tide and Q6DW-GW modulations.
2. A 21 hr secondary wave peaking on September 21 with an amplitude in excess of 40 m/s is observed as the direct confirmation of Q6DW-diurnal tide nonlinear interaction. This wave also appears to be responsible for the subsequent amplification of the Q6DW by in-turn interacting with diurnal tides.
3. The Q6DW clearly modules the GW variances, which provides an additional mechanism of producing the reported ionospheric 6-day variability. The 4–5 days periodicity in GW variances occurs simultaneously with the period shift of Q6DW from 6–7 days to 4–6 days. The mechanism of this connection remains unclear and therefore requires additional studies.
4. The first result of meteor radar observed E-P flux of the Q6DW is presented. The enhanced Q6DW E-P flux indicates potential energy transfer from the mean flow to the Q6DW, which may facilitate the global perturbation and persistence of the Q6DW for an extended time period following the 2019 SH SSW.

The above results lead us to conclude that the presented Q6DW-diurnal tide and Q6DW-GW modulations and interactions appear to have an important impact on the MLT region dynamics, and contribute to facilitating the coupling between the Q6DW and the reported ionospheric 6-day variability. It is also interesting to further investigate the fundamental wave-wave interactions across the scales of planetary waves, tides, and gravity waves, with or without the SSW events.

Data Availability Statement

The CONDOR and Buckland Park MR data utilized in the current study have been uploaded to the NSF CEDAR madrigal database (A. Z. Liu, 2019). To access the data, follow these steps: select “Access Data,” then “List

Experiments," choose "Meteor Radars" from the list of "Choose instrument category(s)" and find "CONDOR [2019–2020]" under "Choose instrument(s)." The data used to produce figures in this letter is available at Qiao et al. (2023).

Acknowledgments

Z. Qiao acknowledges the discussions with Ruth Lieberman, Yosuke Yamazaki, Quan Gan, and Maosheng He. A. Z. Liu and Z. Qiao thank AURA, LCO, and SCO team for the excellent infrastructure support of CONDOR deployment. A. Z. Liu is currently supported by (while serving at) the National Science Foundation (NSF), USA. These results are partly based upon work supported by the NSF National Center for Atmospheric Research (NCAR), which is a major facility sponsored by the NSF under Cooperative Agreement No. 1852977 (N. M. Pedatella). Z. Qiao and J. Fuentes are supported by NSF Grant AGS-1828589. Z. Qiao was also partly supported by NSF NCAR's Advanced Study Program graduate student fellowship. Any opinions, findings and conclusions or recommendations expressed in this material do not necessarily reflect the views of the NSF. G. Stober is member of the Oeschger Center for Climate Change Research (OCCR). The 3DVAR retrievals were developed as part of the ARISE design study (http://arise-project.eu/, last access: 22 November 2022) funded by the European Union's Seventh Framework Programme for Research and Technological Development. The Buckland Park MR ST/meteor radar and the Buckland Park field site are supported by ATRAD Pty. Ltd. and the University of Adelaide. The involvement of I. M. Reid and C. L. Adami was supported by ATRAD Pty. Ltd.

References

Andrews, D. G., & McIntyre, M. E. (1976). Planetary waves in horizontal and vertical shear: The generalized Eliassen-Palm relation and the mean zonal acceleration. *Journal of the Atmospheric Sciences*, *33*(11), 2031–2048. https://doi.org/10.1175/1520-0469(1976)033⟨2031:PWIHAV⟩2.0.CO;2

Baldwin, M. P., Ayarzagüena, B., Birner, T., Butchart, N., Butler, A. H., Charlton-Perez, A. J., et al. (2021). Sudden stratospheric warmings. *Reviews of Geophysics*, *59*(1), e2020RG000708. https://doi.org/10.1029/2020RG000708

Conte, J. F., Chau, J. L., Liu, A., Qiao, Z., Fritts, D. C., Hormaechea, J. L., et al. (2022). Comparison of MLT momentum fluxes over the Andes at four different latitudinal sectors using multistatic radar configurations. *Journal of Geophysical Research: Atmospheres*, *127*(4), e2021JD035982. https://doi.org/10.1029/2021JD035982

De Wit, R., Janches, D., Fritts, D., & Hibbins, R. (2016). QBO modulation of the mesopause gravity wave momentum flux over Tierra del Fuego. *Geophysical Research Letters*, *43*(8), 4049–4055. https://doi.org/10.1002/2016gl068599

De Wit, R., Janches, D., Fritts, D., Stockwell, R., & Coy, L. (2017). Unexpected climatological behavior of MLT gravity wave momentum flux in the lee of the southern Andes hot spot. *Geophysical Research Letters*, *44*(2), 1182–1191. https://doi.org/10.1002/2016gl072311

De Wit, R. J., Hibbins, R., Espy, P. J., Orsolini, Y., Limpasuvan, V., & Kinnison, D. E. (2014). Observations of gravity wave forcing of the mesopause region during the January 2013 major sudden stratospheric warming. *Geophysical Research Letters*, *41*(13), 4745–4752. https://doi.org/10.1002/2014gl060501

Edmon, H., Jr., Hoskins, B., & McIntyre, M. (1980). Eliassen-palm cross sections for the troposphere. *Journal of the Atmospheric Sciences*, *37*(12), 2600–2616. https://doi.org/10.1175/1520-0469(1980)037<2600:epcsft>2.0.co;2

Eliassen, A., & Palm, E. (1961). On the transfer of energy in stationary mountain waves. *Geofysiske publikationer*, *22*(3), 1–23.

Forbes, J. M., & Zhang, X. (2017). The quasi-6 day wave and its interactions with solar tides. *Journal of Geophysical Research: Space Physics*, *122*(4), 4764–4776. https://doi.org/10.1002/2017ja023954

Fritts, D., Janches, D., Hocking, W., Mitchell, N., & Taylor, M. J. (2012). Assessment of gravity wave momentum flux measurement capabilities by meteor radars having different transmitter power and antenna configurations. *Journal of Geophysical Research*, *117*(D10), D10108. https://doi.org/10.1029/2011jd017174

Gan, Q., Oberheide, J., Yue, J., & Wang, W. (2017). Short-term variability in the ionosphere due to the nonlinear interaction between the 6 day wave and migrating tides. *Journal of Geophysical Research: Space Physics*, *122*(8), 8831–8846. https://doi.org/10.1002/2017JA023947

Gan, Q., Wang, W., Yue, J., Liu, H., Chang, L. C., Zhang, S., et al. (2016). Numerical simulation of the 6 day wave effects on the ionosphere: Dynamo modulation. *Journal of Geophysical Research: Space Physics*, *121*(10), 10103–10116. https://doi.org/10.1002/2016JA022907

Gasperini, F., Jones, M., Harding, B. J., & Immel, T. J. (2022). Direct observational evidence of altered mesosphere lower thermosphere mean circulation from a major sudden stratospheric warming. *Authorea Preprints*.

Geisler, J., & Dickinson, R. E. (1976). The five-day wave on a sphere with realistic zonal winds. *Journal of the Atmospheric Sciences*, *33*(4), 632–641. https://doi.org/10.1175/1520-0469(1976)033<0632:tfdwoa>2.0.co;2

Goncharenko, L. P., Harvey, V. L., Greer, K. R., Zhang, S.-R., & Coster, A. J. (2020). Longitudinally dependent low-latitude ionospheric disturbances linked to the Antarctic sudden stratospheric warming of September 2019. *Journal of Geophysical Research: Space Physics*, *125*(8), e2020JA028199. https://doi.org/10.1029/2020JA028199

He, M., Chau, J. L., Forbes, J. M., Thorsen, D., Li, G., Siddiqui, T. A., et al. (2020). Quasi-10-day wave and semidiurnal tide nonlinear interactions during the southern hemispheric SSW 2019 observed in the northern hemispheric mesosphere. *Geophysical Research Letters*, *47*(23), e2020GL091453. https://doi.org/10.1029/2020gl091453

He, M., Chau, J. L., Hall, C. M., Tsutsumi, M., Meek, C., & Hoffmann, P. (2018). The 16-day planetary wave triggers the SW1-tidal-like signatures during 2009 Sudden Stratospheric Warming. *Geophysical Research Letters*, *45*(22), 12631–12638. https://doi.org/10.1029/2018GL079798

He, M., Chau, J. L., Stober, G., Hall, C. M., Tsutsumi, M., & Hoffmann, P. (2017). Application of manley-rowe relation in analyzing nonlinear interactions between planetary waves and the solar semidiurnal tide during 2009 sudden stratospheric warming event. *Journal of Geophysical Research: Space Physics*, *122*(10), 10–783. https://doi.org/10.1002/2017ja024630

Hedin, A. E. (1991). Extension of the MSIS thermosphere model into the middle and lower atmosphere. *Journal of Geophysical Research*, *96*(A2), 1159–1172. https://doi.org/10.1029/90JA02125

Hocking, W. (2005). A new approach to momentum flux determinations using skiymet meteor radars. In *Annales geophysicae* (Vol. 23, pp. 2433–2439).

Hocking, W. K. (1999). Temperatures using radar-meteor decay times. *Geophysical Research Letters*, *26*(21), 3297–3300. https://doi.org/10.1029/1999GL003618

Hocking, W. K., Thayaparan, T., & Jones, J. (1997). Meteor decay times and their use in determining a diagnostic mesospheric temperature-pressure parameter: Methodology and one year of data. *Geophysical Research Letters*, *24*(23), 2977–2980. https://doi.org/10.1029/97GL03048

Holdsworth, D. A., Reid, I. M., & Cervera, M. A. (2004). Buckland park all-sky interferometric meteor radar. *Radio Science*, *39*(5), 1–12. https://doi.org/10.1029/2003rs003014

Jones, M., Jr., Siskind, D., Drob, D., McCormack, J., Emmert, J., Dhadly, M., et al. (2020). Coupling from the middle atmosphere to the exobase: Dynamical disturbance effects on light chemical species. *Journal of Geophysical Research: Space Physics*, *125*(10), e2020JA028331. https://doi.org/10.1029/2020ja028331

Jucker, M., Reichler, T., & Waugh, D. W. (2021). How frequent are Antarctic sudden stratospheric warmings in present and future climate. *Geophysical Research Letters*, *48*(11), e2021GL093215. https://doi.org/10.1029/2021GL093215

Kaiser, T., & Closs, R. (1952). I. Theory of radio reflections from meteor trails: I. *The London, Edinburgh and Dublin Philosophical Magazine and Journal of Science*, *43*(336), 1–32. https://doi.org/10.1080/14786440108520963

Lee, W., Song, I.-S., Kim, J.-H., Kim, Y. H., Jeong, S.-H., Eswaraiah, S., & Murphy, D. (2021). The observation and SD-WACCM simulation of planetary wave activity in the middle atmosphere during the 2019 southern hemispheric sudden stratospheric warming. *Journal of Geophysical Research: Space Physics*, *126*(6), e2020JA029094. https://doi.org/10.1029/2020ja029094

Lieberman, R., Riggin, D., Franke, S., Manson, A., Meek, C., Nakamura, T., et al. (2003). The 6.5-day wave in the mesosphere and lower thermosphere: Evidence for baroclinic/barotropic instability. *Journal of Geophysical Research*, *108*(D20), 4640. https://doi.org/10.1029/2002jd003349

Lieberman, R., Riggin, D., & Siskind, D. (2013). Stationary waves in the wintertime mesosphere: Evidence for gravity wave filtering by stratospheric planetary waves. *Journal of Geophysical Research: Atmospheres*, *118*(8), 3139–3149. https://doi.org/10.1002/jgrd.50319

Liu, A. Z. (2019). Condor—A multi-static meteor radar [Dataset]. *NSF CEDAR Madrigal Databas*. Retrieved from http://cedar.openmadrigal.org/

Liu, A. Z., Lu, X., & Franke, S. J. (2013). Diurnal variation of gravity wave momentum flux and its forcing on the diurnal tide. *Journal of Geophysical Research: Atmospheres*, *118*(4), 1668–1678. https://doi.org/10.1029/2012jd018653

Liu, G., Janches, D., Lieberman, R. S., Moffat-Griffin, T., Mitchell, N. J., Kim, J.-H., & Lee, C. (2021). Wind variations in the mesosphere and lower thermosphere near 60 degrees s latitude during the 2019 Antarctic sudden stratospheric warming. *Journal of Geophysical Research-Space Physics*, *126*(5), e2020JA028909. https://doi.org/10.1029/2020ja028909

Liu, H.-L. (2016). Variability and predictability of the space environment as related to lower atmosphere forcing. *Space Weather*, *14*(9), 634–658. https://doi.org/10.1002/2016sw001450

Ma, Z., Gong, Y., Zhang, S., Xiao, Q., Xue, J., Huang, C., & Huang, K. (2022). Understanding the excitation of quasi-6-day waves in both hemispheres during the September 2019 Antarctic SSW. *Journal of Geophysical Research: Atmospheres*, *127*(3), e2021JD035984. https://doi.org/10.1029/2021jd035984

Matsuno, T. (1971). A dynamical model of the stratospheric sudden warming. *Journal of the Atmospheric Sciences*, *28*(8), 1479–1494. https://doi.org/10.1175/1520-0469(1971)028<1479:admots>2.0.co;2

McLandress, C., & McFarlane, N. (1993). Interactions between orographic gravity wave drag and forced stationary planetary waves in the winter northern hemisphere middle atmosphere. *Journal of the Atmospheric Sciences*, *50*(13), 1966–1990. https://doi.org/10.1175/1520-0469(1993)050<1966:ibogwd>2.0.co;2

Meyer, C. K. (1999). Gravity wave interactions with mesospheric planetary waves: A mechanism for penetration into the thermosphere-ionosphere system. *Journal of Geophysical Research*, *104*(A12), 28181–28196. https://doi.org/10.1029/1999ja900346

Meyer, C. K., & Forbes, J. M. (1997). A 6.5-day westward propagating planetary wave: Origin and characteristics. *Journal of Geophysical Research*, *102*(D22), 26173–26178. https://doi.org/10.1029/97jd01464

Mitra, G., Guharay, A., Batista, P. P., & Buriti, R. (2022). Impact of the September 2019 minor sudden stratospheric warming on the low-latitude middle atmospheric planetary wave dynamics. *Journal of Geophysical Research: Atmospheres*, *127*(1), e2021JD035538. https://doi.org/10.1029/2021jd035538

Miyoshi, Y., & Yamazaki, Y. (2020). Excitation mechanism of ionospheric 6-day oscillation during the 2019 September sudden stratospheric warming event. *Journal of Geophysical Research: Space Physics*, *125*(9), e2020JA028283. https://doi.org/10.1029/2020ja028283

Oberheide, J., Pedatella, N., Gan, Q., Kumari, K., Burns, A., & Eastes, R. (2020). Thermospheric composition o/n response to an altered meridional mean circulation during sudden stratospheric warmings observed by gold. *Geophysical Research Letters*, *47*(1), e2019GL086313. https://doi.org/10.1029/2019gl086313

Pedatella, N. M., & Forbes, J. M. (2010). Evidence for stratosphere sudden warming-ionosphere coupling due to vertically propagating tides. *Geophysical Research Letters*, *37*(11), L11104. https://doi.org/10.1029/2010GL043560

Pedatella, N. M., Liu, H.-L., & Hagan, M. E. (2012). Day-to-day migrating and nonmigrating tidal variability due to the six-day planetary wave. *Journal of Geophysical Research*, *117*(A6), A06301. https://doi.org/10.1029/2012JA017581

Qiao, Z., Liu, A., Pedatella, N. M., Stober, G., Reid, I. M., Fuentes, J., & Adami, C. L. (2023). Evidence for SSW triggered Q6DW-tide-gravity wave interactions observed by meteor radars at 30°s [Dataset]. *Figshare*. https://doi.org/10.6084/m9.figshare.23713374.v1

Spargo, A. J., Reid, I. M., & MacKinnon, A. D. (2019). Multistatic meteor radar observations of gravity-wave–tidal interaction over southern Australia. *Atmospheric Measurement Techniques*, *12*(9), 4791–4812. https://doi.org/10.5194/amt-12-4791-2019

Stober, G., Brown, P., Campbell-Brown, M., & Weryk, R. (2021). Triple-frequency meteor radar full wave scattering-measurements and comparison to theory. *Astronomy & Astrophysics*, *654*, A108. https://doi.org/10.1051/0004-6361/202141470

Stober, G., Jacobi, C., Fröhlich, K., & Oberheide, J. (2008). Meteor radar temperatures over collm (51.3 n, 13 e). *Advances in Space Research*, *42*(7), 1253–1258. https://doi.org/10.1016/j.asr.2007.10.018

Stober, G., Jacobi, C., Matthias, V., Hoffmann, P., & Gerding, M. (2012). Neutral air density variations during strong planetary wave activity in the mesopause region derived from meteor radar observations. *Journal of Atmospheric and Solar-Terrestrial Physics*, *74*, 55–63. https://doi.org/10.1016/j.jastp.2011.10.007

Stober, G., Janches, D., Matthias, V., Fritts, D., Marino, J., Moffat-Griffin, T., et al. (2021). Seasonal evolution of winds, atmospheric tides, and Reynolds stress components in the southern hemisphere mesosphere–lower thermosphere in 2019. In *Annales geophysicae* (Vol. 39, pp. 1–29).

Stober, G., Kozlovsky, A., Liu, A., Qiao, Z., Tsutsumi, M., Hall, C., et al. (2021). Atmospheric tomography using the Nordic meteor radar cluster and Chilean observation network de meteor radars: Network details and 3d-var retrieval. *Atmospheric Measurement Techniques*, *14*(10), 6509–6532. https://doi.org/10.5194/amt-14-6509-2021

Stober, G., Kuchar, A., Pokhotelov, D., Liu, H., Liu, H.-L., Schmidt, H., et al. (2021). Interhemispheric differences of mesosphere–lower thermosphere winds and tides investigated from three whole-atmosphere models and meteor radar observations. *Atmospheric Chemistry and Physics*, *21*(18), 13855–13902. https://doi.org/10.5194/acp-21-13855-2021

Stober, G., Liu, A., Kozlovsky, A., Qiao, Z., Kuchar, A., Jacobi, C., et al. (2022). Meteor radar vertical wind observation biases and mathematical debiasing strategies including the 3DVAR+ DIV algorithm. *Atmospheric Measurement Techniques*, *15*(19), 5769–5792. https://doi.org/10.5194/amt-15-5769-2022

Teitelbaum, H., & Vial, F. (1991). On tidal variability induced by nonlinear interaction with planetary waves. *Journal of Geophysical Research*, *96*(A8), 14169–14178. https://doi.org/10.1029/91ja01019

Wang, J., Palo, S., Forbes, J., Marino, J., Moffat-Griffin, T., & Mitchell, N. (2021). Unusual quasi 10-day planetary wave activity and the ionospheric response during the 2019 southern hemisphere sudden stratospheric warming. *Journal of Geophysical Research: Space Physics*, *126*(6), e2021JA029286. https://doi.org/10.1029/2021ja029286

Yamazaki, Y., & Matthias, V. (2019). Large-amplitude quasi-10-day waves in the middle atmosphere during final warmings. *Journal of Geophysical Research: Atmospheres*, *124*(17–18), 9874–9892. https://doi.org/10.1029/2019jd030634

Yamazaki, Y., Matthias, V., Miyoshi, Y., Stolle, C., Siddiqui, T., Kervalishvili, G., et al. (2020). September 2019 Antarctic sudden stratospheric warming: Quasi-6-day wave burst and ionospheric effects. *Geophysical Research Letters*, *47*(1), e2019GL086577. https://doi.org/10.1029/2019gl086577

Yi, W., Xue, X., Chen, J., Dou, X., Chen, T., & Li, N. (2016). Estimation of mesopause temperatures at low latitudes using the Kunming meteor radar. *Radio Science*, *51*(3), 130–141. https://doi.org/10.1002/2015rs005722